Spin-isospin excitations in the direction of β^+ decay for ^{80}Zn and ^{126}Ru at finite temperature

L. Guo [1,2] W. L. Lv [1,2] Y. F. Niu [1,2,*] D. L. Fang [3,4] B. S. Gao,[3,4] K. A. Li,[3,4] and X. D. Tang [3,4]

[1]*School of Nuclear Science and Technology, Lanzhou University, Lanzhou 730000, China*
[2]*Frontiers Science Center for Rare isotopes, Lanzhou University, Lanzhou 730000, China*
[3]*Institute of Modern Physics, Chinese Academy of Sciences, Lanzhou 730000, China*
[4]*School of Nuclear Science and Technology, University of Chinese Academy of Sciences, Beijing 100049, China*

(Received 1 September 2022; revised 7 November 2022; accepted 9 December 2022; published 23 January 2023)

We investigate the Gamow-Teller (GT) and spin-dipole (SD) transitions in the direction of β^+ decay for neutron-rich $N = 50$ nucleus ^{80}Zn and $N = 82$ nucleus ^{126}Ru, which are important for deleptonization phase in core-collapse supernova, at $T = 0,\ 1,\ 2$ MeV with finite-temperature proton-neutron relativistic (quasiparticle) random-phase approximation. At zero temperature, the GT$^+$ transitions for ^{80}Zn and ^{126}Ru are almost completely Pauli blocked because one more extra shell is occupied for neutrons than that for protons. With increasing temperature to even 2 MeV, the thermal excitation still cannot open up GT$^+$ transitions with strong strength. The SD$^+$ transitions in ^{80}Zn are mildly affected by temperature, which means the experimental data measured at the laboratory can provide useful information for transitions in an astrophysical environment. However, for SD$^+$ transitions in ^{126}Ru, the transition energies have a decrease of about 2 MeV from zero temperature to $T = 1$ MeV due to the collapse of pairing gap of transition orbitals. The total strength in T^+ channel decreases with increasing temperature for both GT and SD transitions, due to the suppression of their transition strength induced by temperature effects.

DOI: 10.1103/PhysRevC.107.014318

I. INTRODUCTION

The nucleus is composed of two kinds of fermions (neutron and proton) with spin and isospin degrees of freedom. The spin-isospin excitations of nuclear systems not only probe the spin-isospin properties of nucleon-nucleon effective interactions [1–3] but also dominate nuclear weak-interaction processes such as β decay [4,5], electron capture [6–8], and neutrino-nucleus scattering [9,10], which are important for understanding the evolution of core-collapse supernova [11,12] and the nucleosynthesis of elements heavier than iron [13].

Spin-isospin excitations of nuclei include different modes according to the changes in quantum numbers, such as Gamow-Teller (GT) excitation and spin-dipole (SD) excitation. The GT resonance, which involves the changes of isospin and spin but the orbital angular momentum remains unchanged ($\Delta S = 1,\ \Delta T = 1,\ \Delta L = 0$), was predicted first by Ikeda, Fujii, and Fujita in 1963 [14], while the first experimental indications of the GT resonance were observed in ^{90}Zr(p, n) change-exchange reactions in 1975 [15]. The low-lying GT strength is connected with β decay and electron capture, since allowed β decay and electron capture take place at essentially momentum transfers $q = 0$ [1]. The SD resonance has an additional one-unit transfer of orbital angular momentum ($\Delta S = 1,\ \Delta T = 1,\ \Delta L = 1$), with three components $\Delta J^\pi = 0^-,\ 1^-,\ 2^-$. This mode was discovered in a ^{208}Pb(p, n) experiment by Horen *et al.* [16], and Gaarde *et al.* [17] further investigated its related properties. SD transitions are first-forbidden transitions in β decay and electron-capture processes.

Experimentally, the spin-isospin excitations can be investigated by β^- decay [18]. However, the energy window of β^- decay experiments are very limited and the strongest states in the spectrum are missed. It is overcome by hadronic probes such as (p, n) or $(^3\mathrm{He}, t)$ [3], and (n, p) charge-exchange reactions [19]. However, the extraction of spin-dipole transition strengths from charge-exchange reaction is also challenging. Therefore, the theoretical study of spin-dipole transitions is necessary, especially for those nuclei that cannot be reached by experiment yet. Theoretically, spin-isospin response can be studied by shell-model (SM) and random-phase approximation (RPA). The SM calculations can provide good agreements with the experimental data [20–23] in the mass region $A \leqslant 70$ or heavier nuclei near shell closure, while its results are difficult to extend beyond the pf shell due to the huge configuration space required. The RPA approach is not limited by configuration space and provides a unified description of all nuclei in nuclear chart except for a few light nuclei [24,25].

In the context of nuclear astrophysics, temperature effects become important for spin-isospin excitations of nuclei. For instance, during the core-collapse of massive stars, the typical temperature at which electron capture occurs is about $T = 1$ MeV [26,27]. Therefore, temperature effects have to be considered in the description of spin-isospin excitations. Based on Skyrme density functionals, the fully self-consistent finite-temperature proton-neutron RPA (FT-PNRPA) was developed to study spin-dipole excitations at finite temperature

*niuyf@lzu.edu.cn

and electron-capture rates [28,29]. Below the critical temperature $T_c \simeq 0.5$–$0.6\Delta_{T=0}$ ($\Delta_{T=0}$ is the pairing gap at zero temperature), the pairing collapse does not occur [30–32], and the pairing correlations would make the Fermi surface of the open-shell nucleus diffuse, which is important for the spin-isospin excitations of the nucleus. To further consider the pairing correlations in open-shell nuclei, the finite-temperature quasiparticle RPA (FT-QRPA) [33,34] and the thermal quasiparticle RPA (TQRPA) [27,35] based on Skyrme density functionals were developed. Recently, a more advanced model which includes particle vibration coupling has also been developed [36].

Covariant density-functional theory (CDFT) has achieved great success in describing the nuclear ground-state and excited properties with only a few parameters [37,38]. Within this framework, the finite-temperature proton-neutron relativistic RPA (FT-PNRRPA) approach was developed in Ref. [8], which was applied to calculate spin-isospin excitations in hot nuclei and electron-capture rates. Furthermore, finite-temperature proton-neutron relativistic quasiparticle RPA (FT-PNRQRPA) [39] was used to calculate electron-capture rates and the temperature evolution of β-decay half-lives [40,41].

During core collapse, electron capture is dominated by the T^+ channel of GT (GT^+) transitions, and the contributions from first-forbidden spin-dipole (SD) transitions become important at higher densities or temperatures [26,42]. However, various recent works have shown the insufficient understanding of electron-capture processes, which has an impact on the dynamics of core collapse, such as the mass of the inner core at bounce and the neutrino luminosity peak [43–47]. References [43,48] have pointed out that the nuclei with the primary contributors to the deleptonization during core collapse are the neutron-rich nuclei close to the $N = 50$ and $N = 82$ neutron closed shell. The contribution to the reduction of electron fraction $Y_e(= Z/A)$ for individual nuclei relates to the product of its electron-capture rate and its abundance. However, there is not much information about these nuclei, both theoretically and experimentally. Sullivan *et al.* [43] and Pascal *et al.* [49] pointed out that the electron-capture rates for nuclei close to the $N = 50$ neutron closed shell are overestimated by the single-state approximation, and the $N = 50$ neutron shell gap could act as a hindrance for stellar electron capture. This conclusion was supported by the experimental measurements of GT^+ strength distributions for the ground state in the $N = 50$ nuclei ^{86}Kr [50] and ^{88}Sr [51]. However, the calculations of TQRPA [27], hybrid model [42], and FT-QRPA [52] indicate that the Pauli blocking of GT strength for nuclei around $N = 50$ can be overcome by thermal excitations under core-collapse conditions. Furthermore, both models predict sizable contributions to the electron capture from SD transitions [27,42,52]. Therefore, theoretical and experimental studies on the spin-isospin excitations of nuclei around $N = 50$ are still insufficient, and even less for nuclei around $N = 82$, due to the neutron-rich nature of these nuclei.

In this work, the self-consistent proton-neutron relativistic QRPA (PNRQRPA) [53–55] is used to investigate the GT and SD transitions in the direction of β^+ decay of ^{80}Zn and ^{126}Ru with $N = 50$ and $N = 82$ neutron closed shells, respectively, which are among those nuclei that mainly contribute to the deleptonization phase of collapse [43]. According to Ref. [56], ^{80}Zn becomes most abundant at $T = 16.76$ GK (1.44 MeV). When $T = 23.2$ GK (2 MeV), ^{126}Ru may also exist in the collapsing core. The pairing correlations can be ignored for temperatures above the critical temperature, which typically amounts to 0.5–1.0 MeV in medium-heavy nuclei [30,31,36,57,58], and hence we adopt FT-PNRPA using relativistic density functional to study the T^+ channel of GT and SD transitions in ^{80}Zn and ^{126}Ru at $T = 1$ and 2 MeV, in order to see in detail how temperature effects play its role in spin-isospin excitations, which could give us clues about possible influences on electron-capture study.

The paper is organized as follows: In Sec. II the framework of PNRQRPA and FT-PNRRPA are introduced. The GT and SD strength distributions at zero temperature and finite temperatures are discussed in Sec. III. Section IV summarizes the present work.

II. THEORETICAL FRAMEWORK

A. Proton-neutron relativistic quasiparticle random-phase approximation

The relativistic QRPA (RQRPA) equation can be derived from the time-dependent relativistic Hartree-Bogoliubov (RHB) model by using the small-amplitude approximation [53]. For transitions between spherical even-even parent nucleus with the 0^+ ground state and the corresponding odd-odd daughter nucleus with J^π excited state, the matrix equations of PNRQRPA in the form of angular momentum coupling read

$$\begin{pmatrix} \mathcal{A}^J_{pn,p'n'} & \mathcal{B}^J_{pn,p'n'} \\ -\mathcal{B}^J_{pn,p'n'} & -\mathcal{A}^J_{pn,p'n'} \end{pmatrix} \begin{pmatrix} X^{\nu J}_{p'n'} \\ Y^{\nu J}_{p'n'} \end{pmatrix} = E_\nu \begin{pmatrix} X^{\nu J}_{pn} \\ Y^{\nu J}_{pn} \end{pmatrix}. \quad (1)$$

The matrix elements of $\mathcal{A}^J$ and $\mathcal{B}^J$ are calculated based on the canonical basis,

$$\mathcal{A}^J_{pn,p'n'} = H^{11}_{pp'}\delta_{nn'} + H^{11}_{nn'}\delta_{pp'} + (u_p v_n u_{p'} v_{n'} + v_p u_n v_{p'} u_{n'}) \times V^{PHJ}_{pn'np'} + (u_p u_n u_{p'} u_{n'} + v_p v_n v_{p'} v_{n'}) V^{PPJ}_{pnp'n'}, \quad (2)$$

$$\mathcal{B}^J_{pn,p'n'} = (u_p v_n v_{p'} u_{n'} + v_p u_n u_{p'} v_{n'}) V^{PHJ}_{pn'np'} - (u_p u_n v_{p'} v_{n'} + v_p v_n u_{p'} u_{n'}) V^{PPJ}_{pnp'n'}. \quad (3)$$

The proton and neutron canonical states are denoted by p, p', and n, n', respectively. The occupation amplitudes $u_{p,n}$ and $v_{p,n}$ are eigenvalues of the density matrix diagonalized in canonical basis. The matrix elements $H^{11}_{nn'}$ and $H^{11}_{pp'}$ are composed of a Dirac single-nucleon mean-field Hamiltonian $\hat{h}_D$, obtained from the variation of energy functional with respect to Hermitian density matrix and the pairing field $\hat{\Delta}$. The matrix elements $H^{11}_{\kappa\kappa'}$ (with $\kappa\kappa' = pp'$ or nn') read

$$H^{11}_{\kappa\kappa'} = (u_\kappa u_{\kappa'} - v_\kappa v_{\kappa'}) h_{\kappa\kappa'} - (u_\kappa v_{\kappa'} + v_\kappa u_{\kappa'}) \Delta_{\kappa\kappa'}. \quad (4)$$

In the PNRQRPA equation, E_ν is the eigenenergy of the excited state $|\nu J\rangle$. $X^{\nu J}$ and $Y^{\nu J}$ are the corresponding forward- and backward-going QRPA two-quasiparticle amplitudes, respectively. V^{PH} is the particle-hole residual two-body interaction between proton and neutron, derived from the

Lagrangian density with medium-dependent meson-nucleon couplings which is the same as that adopted in the RHB model except the terms generated by π mesons. In the RHB calculation, the contribution from π mesons is not present without the inclusion of the Fock term due to parity conservation. However, it is important for the excited states involving the spin degrees of freedom. For charge-exchange transition, since isospin is almost conserved, the residual interaction V^{PH} are only generated by isovector mesons π and ρ. Furthermore, the rearrangement terms introduced by the explicit density dependence of the meson-nucleon couplings are absent in the charge-exchange channel because coupling strengths only depend on the isoscalar ground-state density. The strength parameter g' in zero-range Landau-Migdal term is determined by reproducing experimental data on the GT resonance excitation energy of ^{208}Pb. For effective interaction DD-ME2 [59], the parameter g' is taken as 0.52. V^{PP} is the proton-neutron particle-particle residual interaction, where the Gogny pairing force [60] is adopted. For the $T = 1$ channel, the same pairing interaction set D1S [60] is used as proton-proton and neutron-neutron pairing interactions in the particle-particle channel of the RHB model [54]. The $T = 0$ pairing usually plays its roles on the low-lying transition strength functions; for example, it increases the low-lying strength of GT transitions in the direction of β^- decay [54,61,62]. For these very neutron-rich nuclei studied in this work, we tested that the $T = 0$ pairing also changes the low-lying strength of GT and SD transitions, but with a very slight amount. Therefore, the $T = 0$ pairing channel is ignored in the presented results for simplicity.

The transition strengths for the spin-isospin operator $\boldsymbol{T}^J$ are calculated through

$$B^{\nu J}(T^-) = \left| \sum_{pn} \langle p||\boldsymbol{T}^J||n\rangle \left(X^{\nu J}_{pn} u_p v_n + Y^{\nu J}_{pn} v_p u_n\right) \right|^2 \tag{5}$$

in the T^- channel, and

$$B^{\nu J}(T^+) = \left| \sum_{pn} \langle p||\boldsymbol{T}^J||n\rangle \left(X^{\nu J}_{pn} v_p u_n + Y^{\nu J}_{pn} u_p v_n\right) \right|^2 \tag{6}$$

in the T^+ channel, respectively.

B. Finite-temperature proton-neutron relativistic random-phase approximation

The self-consistent FT-PNRRPA based on the finite-temperature relativistic mean-field model has been proposed for the study of charge-exchange transitions in a stellar environment [8]. The framework of finite-temperature relativistic mean-field (FT-RMF) model was introduced in Ref. [63], based on the nonlinear effective interaction NL3 [64]. However, in the present theoretical framework, the relativistic energy density functional with medium-dependent meson-nucleon couplings is adopted [8,65]. In FT-RMF theory, the temperature dependent mean-field equation can be derived by minimization of thermodynamical potential, which retain the same form as that of the relativistic mean-field (RMF) equations for the static case. For a given temperature T, the temperature-dependent mean-field equation can be solved self-consistently, and we could obtain the characteristic properties of the nuclear thermal state; that is, the single-nucleon basis and thermal occupation probabilities $f_{p(n)}$, which represents a Fermi-Dirac distribution,

$$f_{p(n)} = \frac{1}{1 + \exp\left(\frac{\varepsilon_{p(n)} - \mu_{p(n)}}{kT}\right)}, \tag{7}$$

where $\varepsilon_{p(n)}$ is single-nucleon energy, and $\mu_{p(n)}$ is the chemical potential determined by the conservation of the number of nucleons $\sum_{p(n)}(2j_{p(n)} + 1)f_{p(n)} = Z(N)$, where $j_{p(n)}$ is the angular momentum of the single particle. The above single-nucleon basis and thermal occupation factors are used as inputs to RPA calculation. The corresponding FT-PNRRPA equation derived using the single-nucleon basis of FT-RMF model has the same general form as Eq. (1), but with different matrix $\mathcal{A}^J$ and $\mathcal{B}^J$, which read

$$\mathcal{A}^J_{pnp'n'} = (\varepsilon_P - \varepsilon_H)\delta_{pp'}\delta_{nn'} + (\tilde{u}_p\tilde{v}_n\tilde{u}_{p'}\tilde{v}_{n'} + \tilde{v}_p\tilde{u}_n\tilde{v}_{p'}\tilde{u}_{n'}) \times (|f_{n'} - f_{p'}|)V^{PHJ}_{pn'np'}, \tag{8}$$

$$\mathcal{B}^J_{pnp'n'} = (\tilde{u}_p\tilde{v}_n\tilde{v}_{p'}\tilde{u}_{n'} + \tilde{v}_p\tilde{u}_n\tilde{u}_{p'}\tilde{v}_{n'})(|f_{p'} - f_{n'}|)V^{PHJ}_{pn'np'}. \tag{9}$$

$\varepsilon_P - \varepsilon_H$ is the difference between the single-particle energies of particle-like and hole-like states. In FT-PNRRPA, $\varepsilon_P - \varepsilon_H$ could be either $\varepsilon_p - \varepsilon_{\bar{n}}$ or $\varepsilon_n - \varepsilon_{\bar{p}}$, where p (n) denote a proton (neutron) state. The particle-like (hole-like) states of protons and neutrons are represented by p ($\bar{p}$), n ($\bar{n}$), respectively. For a given proton-neutron pair configuration, the particle-like state is defined as the state with a lower occupation probability, while the hole-like state is defined as the one with a higher occupation probability. To ensure the completeness of configuration space, the proton-neutron pairs formed by the fully or partially occupied states in Fermi sea and the empty negative-energy states in the Dirac sea are also considered. The factors $\tilde{u}$ and $\tilde{v}$ are introduced to distinguish the transitions in the T^- and T^+ channels,

$$\tilde{u}_p = 0, \quad \tilde{v}_p = 1, \quad \tilde{u}_n = 1, \quad \tilde{v}_n = 0, \text{ when } f_p > f_n \ (\bar{p}n), \tag{10}$$

$$\tilde{u}_p = 1, \quad \tilde{v}_p = 0, \quad \tilde{u}_n = 0, \quad \tilde{v}_n = 1, \text{ when } f_p < f_n \ (p\bar{n}). \tag{11}$$

The particle-hole residual interaction $V^{PHJ}_{pn'np'}$ is the same as that used in PNRQRPA. After diagonalizing the FT-PNRRPA matrix, one can obtain the excitation energies E_ν and the corresponding forward- and backward-going RPA amplitudes $X^{\nu J}$ and $Y^{\nu J}$, respectively. At finite temperature, the normalization for $X^{\nu J}$ and $Y^{\nu J}$ reads [8]

$$\sum_{pn} \left[\left(X^{\nu J}_{pn}\right)^2 - \left(Y^{\nu J}_{pn}\right)^2\right](|f_p - f_n|) = 1. \tag{12}$$

The transition strength induced by the spin-isospin operator $\boldsymbol{T}^J$ for T^- channel and T^+ channel can be calculated as follows:

$$B^{\nu J}(T^-) = \left| \sum_{pn} \left(X^{\nu J}_{pn}\tilde{u}_p\tilde{v}_n + Y^{\nu J}_{pn}\tilde{v}_p\tilde{u}_n\right)\langle p||\boldsymbol{T}^J||n\rangle(|f_n - f_p|)\right|^2, \tag{13}$$

$$B^{\nu J}(T^+) = \left| \sum_{pn} \left(X^{\nu J}_{pn}\tilde{v}_p\tilde{u}_n + Y^{\nu J}_{pn}\tilde{u}_p\tilde{v}_n\right)\langle p||\boldsymbol{T}^J||n\rangle(|f_n - f_p|)\right|^2. \tag{14}$$

C. Non-energy-weighted sum rule for Gamow-Teller and spin-dipole transitions

For the $T^\pm$ channels of GT transition, the spin-isospin operator reads [1]

$$\boldsymbol{T}^\pm(\mathrm{GT}) = \sum_{i=1}^{A} \boldsymbol{\sigma}(i)\tau_\pm(i), \tag{15}$$

with the isospin operators $\tau_3 = \tau_z$, $\tau_\pm = (\tau_x \pm i\tau_y)$, and $\boldsymbol{\sigma}$ denotes the spin operator, whose three components in spherical coordinates are

$$\sigma_\pm = \mp\frac{1}{\sqrt{2}}(\sigma_x \pm i\sigma_y), \tag{16}$$

$$\sigma_0 = \sigma_z. \tag{17}$$

Based on the commutation relation $[\tau_+, \tau_-] = \tau_3$ and the properties of tensor operator $\boldsymbol{\sigma}$, one can obtain the non-energy-weighted sum rule for the GT transition:

$$\begin{aligned} S^{\mathrm{GT}}_- - S^{\mathrm{GT}}_+ &= \sum_\nu B^\nu_-(\mathrm{GT}) - \sum_\nu B^\nu_+(\mathrm{GT}) \\ &= 3(N - Z), \end{aligned} \tag{18}$$

where $S^{\mathrm{GT}}_\pm$ is the total transition strength for the $T^\pm$ channels of the GT transition. For the charge-exchange SD transition, it has three components $\Delta J^\pi = 0^-, 1^-, 2^-$ induced by the tensor operator [17]

$$\boldsymbol{T}^\pm(\mathrm{SD}) = \sum_i r_i[\boldsymbol{\sigma}(i) \otimes \boldsymbol{Y}_1(i)]_{J=0,1,2}\tau_\pm(i). \tag{19}$$

The non-energy-weighted sum rule for SD transition as well as its three components can be written as [66,67]

$$\begin{aligned} S^{\mathrm{SD}}_{-,\mathrm{tot.}} - S^{\mathrm{SD}}_{+,\mathrm{tot.}} &= \sum_{\nu J} B^{\nu J}_-(\mathrm{SD}) - \sum_{\nu J} B^{\nu J}_+(\mathrm{SD}) \\ &= \frac{9}{4\pi}[N\langle r_n\rangle^2 - Z\langle r_p\rangle^2], \end{aligned} \tag{20}$$

$$\begin{aligned} S^{\mathrm{SD}}_{-,J} - S^{\mathrm{SD}}_{+,J} &= \sum_\nu B^{\nu J}_-(\mathrm{SD}) - \sum_\nu B^{\nu J}_+(\mathrm{SD}) \\ &= \frac{2J+1}{4\pi}[N\langle r_n\rangle^2 - Z\langle r_p\rangle^2], \end{aligned} \tag{21}$$

where $S^{\mathrm{SD}}_{\pm,\mathrm{tot.}}$ is the total strength including the summation of three different J^π components for the $T^\pm$ channels of the SD transition, and $S^{\mathrm{SD}}_{\pm,J}$ is the total transition strength for the $T^\pm$ channel of the corresponding three components. $\langle r_n\rangle$ and $\langle r_p\rangle$ represent the rms radii of neutron and proton distributions, respectively.

III. RESULTS AND DISCUSSION

In this section we present the results of the GT^+ and SD^+ transition strengths for ^{80}Zn and ^{126}Ru at temperatures $T = 0$, 1, and 2 MeV. Since pairing correlations have to be taken into account for open-shell nuclei at zero temperature, the QRPA based on RHB model with the finite-range Gogny pairing force is used in the corresponding calculations. The critical temperature range for nuclear phase transition from superfluid to normal state is around 0.5–1 MeV [30,31,36,57,58]. Therefore, the FT-PNRRPA, which does not include pairing correlations, can provide a reasonable description of GT^+ and SD^+ transitions [8] for the temperature range considered in the present paper ($T = 1$ and 2 MeV). The RHB equation and FT-RMF equation are both solved based on the spherical harmonic-oscillator basis, and 20 oscillator shells are included in our calculation. In the PNRQRPA and FT-PNRRPA models, the maximum energy cutoffs for configurations from the Fermi sea and from the Dirac sea are taken as 100 and 2000 MeV, respectively, and the minimum cutoff on the product of the occupation factors, which means u_pv_n or u_nv_p in PNRQRPA or $\sqrt{f_p(1-f_n)}$ or $\sqrt{f_n(1-f_p)}$ in FT-PNRRPA, is set to be 0.01.

A. The T^+ channel of Gamow-Teller and spin-dipole transitions at $T = 0$ MeV

In Fig. 1(a) we display the GT^+ strength distribution of ^{80}Zn at zero temperature. To analyze the single-particle transition configurations of transition state in ^{80}Zn, we also plot its single-particle energy levels in Fig. 1(b). First, from Fig. 1(a) it can be seen that GT^+ transitions are generally with extremely low strengths, because possible transition channels are Pauli blocked for this very-neutron-rich nucleus. The whole pf neutron shell between $N = 28$–50 is fully occupied, and the available orbitals are from sdg shell above $N = 50$ shell closure, while for protons the sdg shell is almost completely empty, except for a small occupation for the intruder orbital $\pi 1g_{9/2}$ below $Z = 50$ shell closure. Considering the selection rule of GT^+ transitions, almost all transition channels of the same node are blocked with the only possibility for the intruder orbital $\pi 1g_{9/2} \to \nu 1g_{7/2}$. Here we use π (ν) denote proton (neutron). In detail, transitions from $\pi 1f_{7/2,5/2}$ to $\nu 1f_{5/2}$, which should give strong strengths, cannot proceed because the latter orbital has been fully occupied, as marked by the red arrows in Fig. 1(b). Other possible transition channels are also blocked, such as transition $\pi 1g_{9/2} \to \nu 1g_{9/2}$. The $\pi 1g_{9/2}$ orbital above the Fermi surface is partially occupied due to pairing correlations. However, the $\nu 1g_{9/2}$ orbital is fully occupied due to the existence of $N = 50$ shell gap which makes pairing scattering not possible, and hence the transition $\pi 1g_{9/2} \to \nu 1g_{9/2}$ cannot occur, while the transition $\pi 1g_{9/2} \to \nu 1g_{7/2}$ with relatively higher excitation energy can proceed and give rise to the peak A in Fig. 1(a). The transitions from $\pi 2p_{1/2,3/2}$ orbitals, which are partially occupied due to pairing correlations, into $\nu 2p_{1/2,3/2}$ orbitals are also blocked

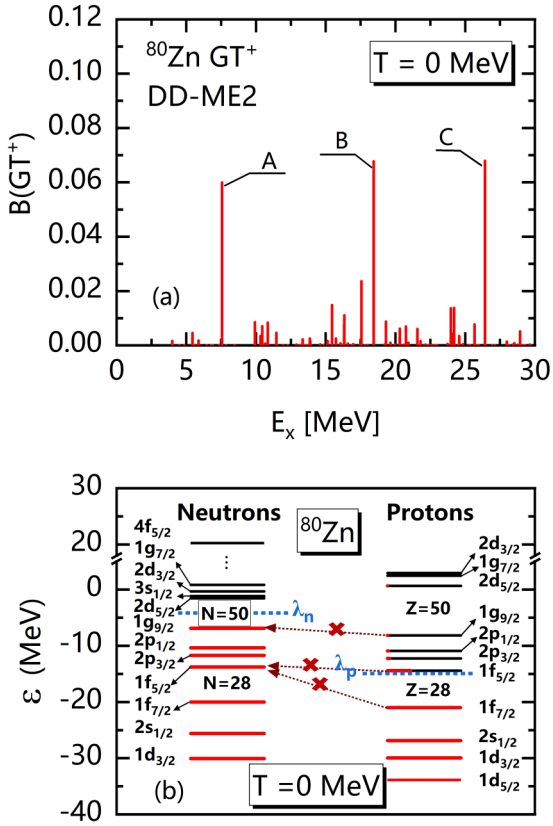

FIG. 1. (a) The GT^+ strength distribution for ^{80}Zn as a function of the excitation energy with respect to the ground state of the daughter nucleus ^{80}Cu, calculated with PNRQRPA at zero temperature for the DD-ME2 relativistic density functional. (b) The single-particle energy levels of ^{80}Zn calculated with DD-ME2 relativistic functional at zero temperature. The left (right) part refers to the neutrons (protons). A, B, and C in panel (a) label the main excitation states with dominant single-particle transitions $\pi 1g_{9/2} \to \nu 1g_{7/2}$ (A), $\pi 1d_{5/2} \to \nu 2d_{3/2}$ (B), and $\pi 1f_{7/2} \to \nu 4f_{5/2}$ (C), respectively. The blocked transitions $\pi 1f_{7/2,5/2} \to \nu 1f_{5/2}$ and $\pi 1g_{9/2} \to \nu 1g_{9/2}$ are denoted by red dashed arrows in panel (b).

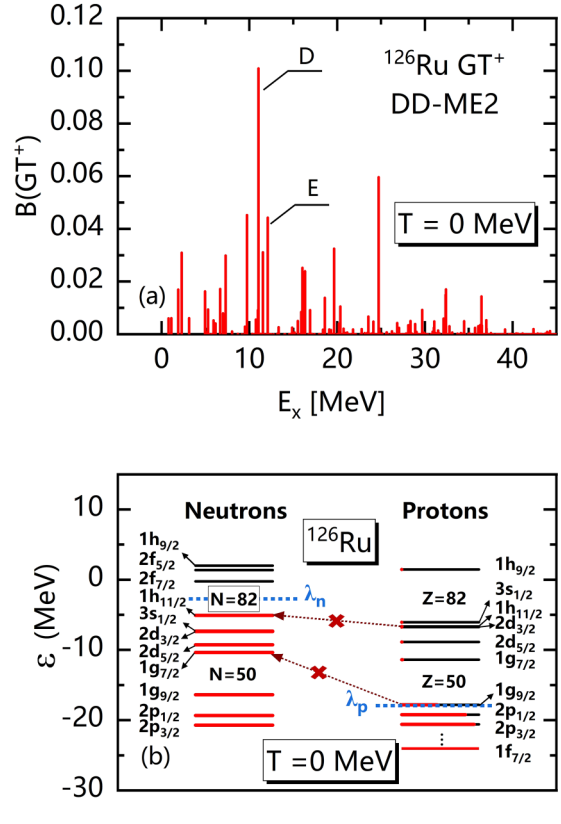

FIG. 2. Same as Fig. 1, but for the nucleus ^{126}Ru. D and E label states with dominated single-particle transitions $\pi 1f_{7/2} \to \nu 2f_{5/2}$ (D) and $\pi 1h_{11/2} \to \nu 1h_{9/2}$ (E), respectively.

for the same reason as the transition $\pi 1g_{9/2} \to \nu 1g_{9/2}$. Therefore, the calculated GT^+ transition spectra with low transition strengths are due to the Pauli blocking effect.

From Fig. 1(a), three main peaks can be observed, which reside at 7.56, 18.44, and 26.40 MeV, respectively. By analyzing the $X^2_{\pi\nu} - Y^2_{\pi\nu}$ of these three excited states, we find their dominant components are transitions $\pi 1g_{9/2} \to \nu 1g_{7/2}$, $\pi 1d_{5/2} \to \nu 2d_{3/2}$, and $\pi 1f_{7/2} \to \nu 4f_{5/2}$ for states at $E_x =$ 7.56, 18.44, and 26.40 MeV, respectively, which are marked by A, B, and C in Fig. 1(a), correspondingly. For peak A formed by the transition $\pi 1g_{9/2} \to \nu 1g_{7/2}$, protons can be scattered into $\pi 1g_{9/2}$ by pairing correlations, enabling GT^+ transitions into $\nu 1g_{7/2}$ orbitals. For peaks B and C located at rather high excitation energies, these excited states are not formed by the unblocking effect of pairing correlations but by the transitions across major shells, and the unperturbed energies E_{unper} of their main transition configurations $\pi 1d_{5/2} \to \nu 2d_{3/2}$ and $\pi 1f_{7/2} \to \nu 4f_{5/2}$ are 18.51 and 26.32 MeV, respectively, which are noticeably larger than that of the transition $\pi 1g_{9/2} \to \nu 1g_{7/2}$, which is 7.55 MeV. For these GT^+ states formed mainly by single-particle transitions, the residual interaction has little effect on them, and the corresponding GT^+ excitation energy is almost the same as the unperturbed energy. It is noticed that, for GT excitations, it is a unit operator in coordinate space, leading to the small strengths of peaks B and C formed by transitions across major shells. In contrast, these transitions across major shells mainly contribute to isovector spin-monopole excitations with r^2 operator in the coordinate space.

The GT^+ transition strength distribution and single-particle energy levels of ^{126}Ru are shown in Figs. 2(a) and 2(b), respectively. Just as the case of ^{80}Zn, GT^+ transition strengths of ^{126}Ru are also very small due to the Pauli blocking effect. Neutrons in ^{126}Ru occupy one more extra shell (*sdg* shell between $N = 50$–82) than protons do, and hence the only possible transition within the same shell is from the intruder orbital $\pi 1h_{11/2} \to \nu 1h_{9/2}$ unblocked by pairing correlations, which gives rise to peak E in Fig. 2(a). Other small transition strengths are formed by transitions across major shells, for instance, from $\pi 2p_{3/2}$ to $\nu 3p_{1/2,3/2}$, $\nu 4p_{1/2}$ orbitals, from $\pi 1f_{5/2}$ to $\nu 2f_{5/2,7/2}$ orbitals, from $\pi 1f_{7/2}$ to $\nu 2f_{5/2,7/2}$ orbitals, and so on, among which, $\pi 1f_{7/2} \to \nu 2f_{5/2}$ gives rise to the highest peak at $E_x = 11.0$ MeV, as marked by D in Fig. 2(a). For transitions within the same major shell, such as $\pi 1g_{9/2} \to \nu 1g_{7/2}$ in ^{80}Zn and $\pi 1h_{11/2} \to \nu 1h_{11/2}$ in ^{126}Ru, are Pauli blocked since their final orbitals $\nu 1g_{7/2}$ and $\nu 1h_{11/2}$

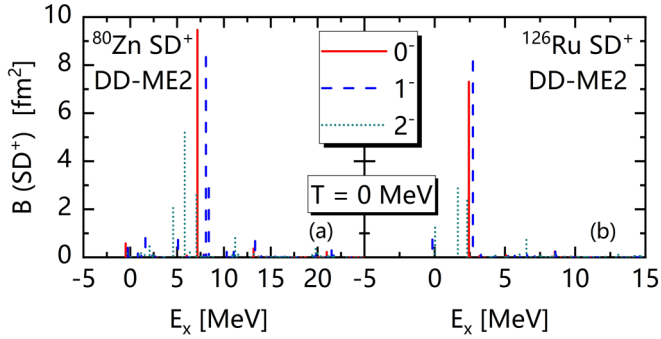

FIG. 3. Spin-dipole transition strength distributions in T^+ channel of ^{80}Zn and ^{126}Ru calculated by PNRQRPA at zero temperature with DD-ME2 interaction. The solid line, dashed line, and dotted line show the 0^-, 1^-, and 2^- components, respectively.

are fully occupied due to the existence of $N = 50$ and 82 shell gaps.

Since the GT$^+$ transitions are almost blocked by the Pauli principle, we next investigate the first-forbidden transition for weak decays, which is a spin-dipole transition. The SD$^+$ transition strength distributions of ^{80}Zn and ^{126}Ru are shown in Fig. 3. It is obvious that relatively strong SD$^+$ transitions appear for both ^{80}Zn and ^{126}Ru. For spin-dipole transitions, the angular-momentum selection rule requires $\Delta L = 1$, thus making SD$^+$ transitions of neutron-rich nuclei possible. For example, transitions $\pi 1f_{7/2} \to \nu 1g_{7/2}, \nu 2d_{3/2}, \pi 1f_{5/2} \to \nu 2g_{7/2}$ in ^{80}Zn, and $\pi 1g_{9/2} \to \nu 1h_{9/2}, \nu 2f_{5/2}$ in ^{126}Ru, as can be seen from Tables I and II are not affected by Pauli blocking and lead to the appearance of SD$^+$ transitions. Besides, SD$^+$ transitions of ^{126}Ru reside at lower energies compared with the case of ^{80}Zn because ^{126}Ru is more neutron rich and hence the ground-state energy difference between mother and daughter nuclei for ^{126}Ru is larger than that for ^{80}Zn.

TABLE I. Excitation energy E_x and transition strength $B(T^+)$ of main excited states of charge-exchange SD transitions of ^{80}Zn shown in Fig. 5, together with their dominant single-particle transitions and the corresponding unperturbed energy $E_{\rm unper}$ (with respect to daughter nucleus), relative RPA norm contribution $X^2_{pn} - Y^2_{pn}$ and reduced transition amplitude A_{pn}. All results are calculated with the DD-ME2 interaction at $T = 0$, 1, and 2 MeV.

T [MeV]	J^π	E_x [MeV]	$B(T^+)$ [fm^2]	Configuration	$E_{\rm unper}$ [MeV]	$X^2_{pn} - Y^2_{pn}$	A_{pn} [fm]
0	0^-	7.16	9.48	$1f_{7/2} \to 1g_{7/2}$	6.88	99.4%	3.20
0	1^-	8.08	8.34	$1f_{7/2} \to 1g_{7/2}$	6.88	74.2%	3.55
0	1^-	8.08	8.34	$1f_{5/2} \to 2g_{7/2}$	8.36	21.8%	−0.12
0	1^-	8.37	2.89	$1f_{5/2} \to 2g_{7/2}$	8.36	72.7%	−0.21
0	1^-	8.37	2.89	$1f_{7/2} \to 1g_{7/2}$	6.88	21.9%	−1.93
0	2^-	5.82	5.19	$1f_{7/2} \to 2d_{3/2}$	5.73	96.5%	−2.13
1	0^-	6.80	9.54	$1f_{7/2} \to 1g_{7/2}$	6.51	99.9%	−3.21
1	1^-	7.77	11.41	$1f_{7/2} \to 1g_{7/2}$	6.51	97.4%	−4.07
1	2^-	5.37	5.13	$1f_{7/2} \to 2d_{3/2}$	5.28	97.6%	2.13
2	0^-	5.76	8.35	$1f_{7/2} \to 1g_{7/2}$	5.49	99.2%	2.98
2	1^-	6.58	10.39	$1f_{7/2} \to 1g_{7/2}$	5.49	95.7%	−3.75
2	2^-	4.22	3.62	$1f_{7/2} \to 2d_{3/2}$	4.13	85.8%	−1.82

TABLE II. Same as Table I, but for the nucleus ^{126}Ru.

T [MeV]	J^π	E_x [MeV]	$B(T^+)$ [fm^2]	Configuration	$E_{\rm unper}$ [MeV]	$X^2_{pn} - Y^2_{pn}$	A_{pn} [fm]
0	0^-	2.43	7.32	$1g_{9/2} \to 1h_{9/2}$	2.24	99.8%	2.91
0	1^-	2.71	8.16	$1g_{9/2} \to 1h_{9/2}$	2.24	99.0%	−3.71
0	2^-	1.64	2.87	$1g_{9/2} \to 2f_{5/2}$	1.61	99.5%	1.77
0	2^-	2.31	2.36	$1g_{9/2} \to 1h_{9/2}$	2.24	99.4%	2.02
1	0^-	0.54	7.23	$1g_{9/2} \to 1h_{9/2}$	0.35	100.0%	−2.90
1	1^-	0.82	7.96	$1g_{9/2} \to 1h_{9/2}$	0.35	100.0%	−3.72
1	2^-	−0.30	2.78	$1g_{9/2} \to 2f_{5/2}$	−0.34	99.6%	−1.78
1	2^-	0.42	2.30	$1g_{9/2} \to 1h_{9/2}$	0.35	99.6%	−2.02
2	0^-	−0.37	6.98	$1g_{9/2} \to 1h_{9/2}$	−0.55	99.5%	−2.83
2	1^-	−0.09	7.00	$1g_{9/2} \to 1h_{9/2}$	−0.55	84.4%	−3.34
2	1^-	−0.09	7.00	$1h_{9/2} \to 3i_{11/2}$	−0.10	14.4%	−0.01
2	1^-	−0.10	1.16	$1h_{9/2} \to 3i_{11/2}$	−0.10	85.6%	−0.01
2	1^-	−0.10	1.16	$1g_{9/2} \to 1h_{9/2}$	−0.55	14.2%	1.37
2	2^-	−1.37	2.45	$1g_{9/2} \to 2f_{5/2}$	−1.40	99.4%	1.70
2	2^-	−0.49	2.34	$1g_{9/2} \to 1h_{9/2}$	−0.55	99.5%	1.97

B. Temperature effects on T^+ channel of Gamow-Teller and spin-dipole transitions

To investigate temperature effects on GT$^+$ transitions, in Figs. 4(a) and 4(c), we plot GT$^+$ strength distributions of ^{80}Zn and ^{126}Ru at $T = 0$, 1, and 2 MeV. In general, GT$^+$ transition energies decrease with increasing temperature. The effects of temperature on nuclear excitations mainly manifest itself in the evolution of single-particle energy levels and occupation factors of neutron and proton orbitals $f_{n(p)}$ [seeing Eq. (7)] that appear in the FT-PNRRPA matrix elements [8]. The evolution of single-particle energy levels directly leads to the change in unperturbed energy $E_{\rm unper}$, while the occupation factor can affect the residual interaction in matrix elements of $\mathcal{A}$ and $\mathcal{B}$. For most transitions in these neutron-rich nuclei, they are simply single-particle transitions across major shells, where the residual interaction plays almost no role on them, so the energy changes with temperature are mainly reflected in their unperturbed energies. From $T = 0$ MeV to $T = 1$ MeV, in principle, pairing collapses due to pairing phase transition, and hence the unperturbed energy should decrease due to the vanishing pairing gap. However, since transitions around Fermi surface with big pairing gaps are almost completely blocked, and the GT$^+$ states are formed by single-particle transitions between orbitals far away from the Fermi surface with small pairing gap, the collapse of pairing correlations has almost no influence on them, and the unperturbed energy from $T = 0$ MeV to $T = 1$ MeV is only changed by a small amount. More obvious changes in unperturbed energy happen from $T = 1$ MeV to $T = 2$ MeV. As an example, one can see for the peak around 25 MeV in ^{80}Zn labeled by C in Fig. 4(a), whose dominant component is $\pi 1f_{7/2} \to \nu 4f_{5/2}$, the unperturbed energies are 26.32, 25.92, and 24.93 MeV with respect to the daughter nucleus for $T = 0$, 1, and 2 MeV, respectively. The same case is found in ^{126}Ru, for example, the state at around 10 MeV labeled by D with dominant single-particle configuration $\pi 1f_{7/2} \to \nu 2f_{5/2}$ in Fig. 4(c). It is noticed that in ^{80}Zn, compared with the higher-energy region, the temper-

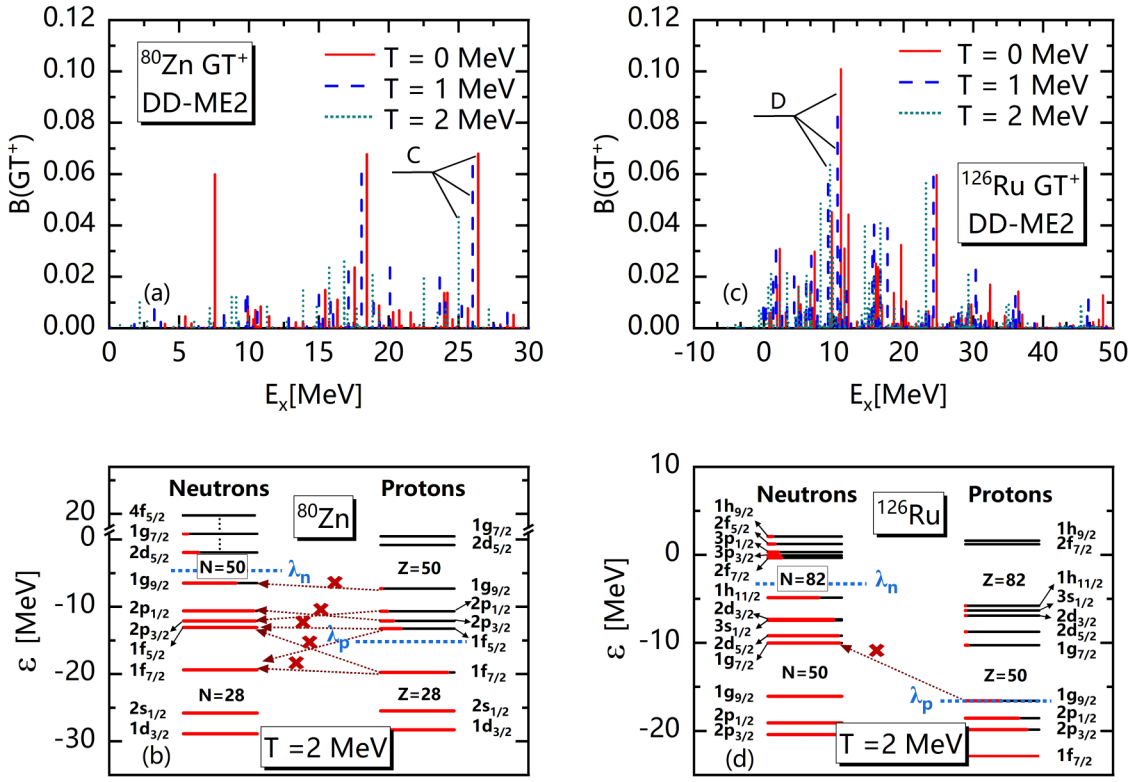

FIG. 4. (a), (c) GT^+ strength distributions of ^{80}Zn and ^{126}Ru, calculated by PNRQRPA at $T = 0$ MeV (solid line) and FT-PNRRPA at $T = 1$ MeV (dashed line) and 2 MeV (dotted line). C and D label GT^+ states with dominant single-particle configurations $\pi 1f_{7/2} \rightarrow \nu 4f_{5/2}$ (C) and $\pi 1f_{7/2} \rightarrow \nu 2f_{5/2}$ (D), respectively. (b), (d) Single-particle energy levels of ^{80}Zn and ^{126}Ru at $T = 2$ MeV. All results are calculated with effective interaction DD-ME2.

ature effects on GT^+ spectra of low-energy region below 5 MeV are bigger. At $T = 1$ MeV some transitions are already shifted below 5 MeV, and they become even lower in energy at $T = 2$ MeV, which may cause a lowering of threshold energy for electron capture. However, these transition strengths are very small, so it is hard to say their possible effects on electron-capture cross sections.

In addition to the excitation energy, instead of thermal unblocking, GT^+ transition strengths become weaker with increasing temperature, and some strengths even vanish at finite temperature. The origin of this temperature dependence results from the smearing of the Fermi surface induced by the variation of the occupation factors $f_{n(p)}$ [8,68]. At zero temperature, there are two types of excitations. One is the transitions formed by unblocking of pairing correlations, like peak A in Fig. 1(a) and peak E in Fig. 2(a), and the other kind is the transitions across different major shells, which are hence not influenced by Pauli blocking, like peaks B and C in Fig. 1(a) and peak D in Fig. 2(a). The first kind of excitations even vanish as the temperature increases, due to changes of occupation probabilities of the corresponding proton and neutron orbitals for these transitions. With increasing temperature, the neutron valence orbitals above the big shell closure can be occupied through thermal excitation, as can be seen in Figs. 4(b) and 4(d), and correspondingly the occupation probabilities of neutron orbitals for transitions A and E, for example, which are 0.006 (1 MeV) and 0.06 (2 MeV) for $\nu 1g_{7/2}$ in ^{80}Zn, become even higher than those of the corresponding proton orbitals, for example, 0.001 (1 MeV) and 0.019 (2 MeV) for $\pi 1g_{9/2}$. The particle-like and hole-like properties of neutron and proton orbitals for this transition are reversed, which makes the forward $\pi 1g_{9/2} \rightarrow \nu$ 1 $g_{7/2}$ transition not possible, and becomes the backward transition in FT-PNRRPA [seeing Eqs. (10) and (11)].

For the second kind of excitations across the major shell, the transition strengths become weaker with increasing temperature. Since these transitions are simply single-particle transitions, the transition strength is determined by the single-particle transition matrix element and the occupation probability difference between the proton and neutron orbitals of this transition. With increasing temperature, the Fermi surface becomes more smeared also for neutrons, leading to a smaller occupation probability difference between the corresponding proton and neutron orbitals, while the single-particle matrix element almost keeps constant with variations of temperature. It is noticed that for these two very neutron-rich nuclei, even at $T = 2$ MeV, the temperature effects still cannot open up new transition channels due to the big difference between proton and neutron Fermi surfaces. The transitions such as $\pi 2p_{1/2,3/2} \rightarrow \nu 2p_{1/2,3/2}$, $\pi 1f_{5/2,7/2} \rightarrow \nu 1f_{5/2,7/2}$, and $\pi 1g_{9/2} \rightarrow \nu 1g_{9/2}$ for ^{80}Zn as well as $\pi 1g_{9/2} \rightarrow \nu 1g_{7/2}$ and so on for ^{126}Ru, as shown by the red dashed arrows in the Figs. 4(b) and 4(d), are still blocked at high temperature.

Figure 5 displays SD^+ transition strength distributions in ^{80}Zn at various temperatures. One can observe that the

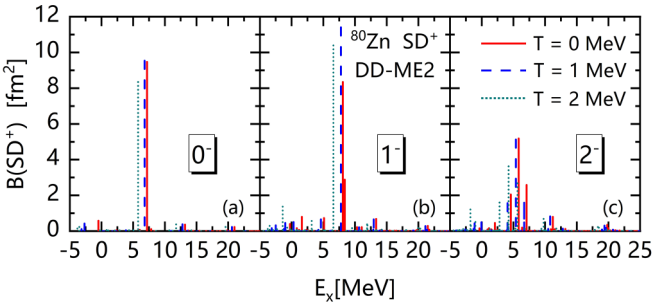

FIG. 5. SD$^+$ transition strength distributions of (a) 0^-, (b) 1^-, and (c) 2^- components in ^{80}Zn at $T = 0$, 1, 2 MeV. The zero-temperature results are calculated by the PNRQRPA, and the finite-temperature results are obtained by FT-PNRRPA. The excitation energy is referred to the ground state of the daughter nucleus ^{80}Cu.

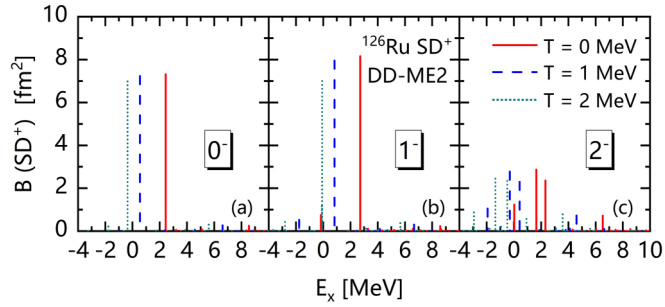

FIG. 6. Same as Fig. 5 but for the nucleus ^{126}Ru.

increased temperature induces a shift of the strength distribution towards lower energies as well as the decrease of transition strengths. However, those changes caused by temperature effects in ^{80}Zn are small, especially for $T = 1$ MeV, which is almost the same as the results obtained at zero temperature. This means that the experimental data measured at ground state of ^{80}Zn can be approximately used for the hot supernova environment. From $T = 0$ MeV to $T = 1$ MeV, the energy shifts for different components of SD transitions are all within 0.5 MeV, as can be seen from Table I, where the excitation energies and transition strength of main peaks, together with their dominant single-particle transitions and corresponding reduced transition amplitude are listed. The reduced transition amplitude A_{pn} in the direction of β^+ decay is calculated with

$$A_{pn} = \langle p||\boldsymbol{T}^J||n\rangle\left(X^{\nu J}_{pn} v_p u_n + Y^{\nu J}_{pn} u_p v_n\right) \tag{22}$$

in PNRQPA and

$$A_{pn} = \langle p||\boldsymbol{T}^J||n\rangle\left(X^{\nu J}_{pn} \tilde{v}_p \tilde{u}_u + Y^{\nu J}_{pn} \tilde{u}_p \tilde{v}_n\right)|f_n - f_p| \tag{23}$$

in FT-PNRRPA according to Eqs. (6) and (14). The reduced transition amplitude contains more information about the transition operator than the relative RPA norm does. For example, for the 1^- state with energy of 8.37 MeV at zero temperature, which has two main configurations, the configuration with a large norm $1f_{5/2} \rightarrow 2g_{7/2}$ actually has a small reduced transition amplitude, leading to a small contribution to the total transition strength. The pairing collapse has no influence on these transitions due to the small pairing gaps of most related transition orbitals that are far from the Fermi surface, just as for the case of GT$^+$. From $T = 1$ MeV to $T = 2$ MeV, the energy shift can reach 1 MeV, mainly due to the changes in unperturbed energy caused by the evolution of single-particle spectra with temperature. As discussed in the case of the GT$^+$ transition, the decreasing of transition strength results from the changes of occupation probability difference between proton and neutron transition orbitals induced by thermal excitation. Let us consider the peak of 0^- state at 7.16 MeV as an example and analyze the evolution behavior of the occupation probabilities of neutron and proton orbitals with temperature. As can be seen from Table I, the peak of 0^- state is mainly contributed by the transition $\pi 1f_{7/2} \rightarrow \nu 1g_{7/2}$. At $T = 0$ and 1 MeV, the occupation probabilities are 0.99 and 1.00 for the proton orbital $\pi 1f_{7/2}$, respectively, while it is always zero for the neutron orbital $\nu 1g_{7/2}$. Therefore, there are almost no changes in the transition strength from 0 to 1 MeV, because the thermal excitations at $T = 1$ MeV are not sufficient to change the occupation of proton orbital $\pi 1f_{7/2}$. However, the occupation probability of proton orbital $\pi 1f_{7/2}$ is 0.91 at $T = 2$ MeV, and it is 0.06 for $\nu 1g_{7/2}$. This results in the decrease of the transition strengths compared with those at $T = 0$ and 1 MeV.

Figure 6 also shows the evolution of SD$^+$ transition strength distributions in ^{126}Ru with temperature. Being different from ^{80}Zn, the energy decrease from $T = 0$ MeV to $T = 1$ MeV is relatively large, and even larger than the decrease from $T = 1$ MeV to $T = 2$ MeV for all the SD components. It means that the pairing collapse plays a role here. From Table II, one can see the proton orbitals of most transitions are $\pi 1g_{9/2}$, which is at Fermi surface, seeing Fig. 2(b), so the pairing gap of this orbital is large (1.50 MeV). After the pairing collapse, this pairing gap vanishes, and it results in the decrease of unperturbed energy. From $T = 1$ MeV to $T = 2$ MeV, the energy shift is about 1 MeV, being similar as that in ^{80}Zn. The evolution of transition strength with temperature is also the same as the case of ^{80}Zn, and the same mechanism plays its role here.

C. Sum rule

To investigate temperature effects on the non-energy-weighted sum rule, we list in Tables III and IV the exhaustion of the non-energy-weighted sum rule obtained with and without contributions from the Dirac sea for ^{80}Zn and ^{126}Ru at various temperatures. The non-energy-weighted sum rules of GT and SD transitions are calculated by Eqs. (18) and (21). Both for ^{80}Zn and ^{126}Ru, obviously the non-energy-weighted sum rule can be almost 100% fulfilled only when the contributions from Dirac sea are included, which are about 3.5%–7%. This confirms the importance of the inclusion of Dirac sea for the fulfillment of sum rule in relativistic calculations [69–71]. However, by comparing the transition strength distributions above the ground-state difference threshold with and without the contributions from Dirac sea, it is found that the transition strengths are the same, and hence the antiparticle contribution is fully decoupled from the particle contribution. For the case without Dirac sea, the non-energy-weighted sum rule

TABLE III. Non-energy-weighted sum-rule values of GT and SD transitions in ^{80}Zn calculated with and without the contributions from Dirac sea at $T = 0$, 1, 2 MeV. The zero-temperature and finite-temperature results are obtained by PNRQRPA and FT-PNRRPA with the DD-ME2 interaction, respectively. S_- and S_+ are the summed strengths of the T^- channel and the T^+ channel, respectively, up to 100 MeV. The column labeled "Sum rule" gives the model-independent nonenergy weighted sum-rule values [14,17]. The exhaustion of the non-energy-weighted sum rule calculated by our model is shown in the last column.

T [MeV]	J^π		S_- [fm^2]	S_+ [fm^2]	$S_- - S_+$ [fm^2]	Sum rule [fm^2]	$\frac{S_- - S_+}{\text{Sum rule}}$ [%]
0	1^+	without	56.4	0.6	55.8	60.0	93.1
0	1^+	with	65.2	5.2	60.1	60.0	100.1
0	0^-	without	42.7	11.4	31.3	33.5	93.3
0	0^-	with	47.1	13.6	33.5	33.5	100.0
0	1^-	without	112.1	16.3	95.8	100.6	95.2
0	1^-	with	122.0	21.3	100.6	100.6	100.0
0	2^-	without	173.4	14.3	159.1	167.7	94.9
0	2^-	with	190.5	22.7	167.7	167.7	100.0
1	1^+	without	56.4	0.5	55.9	60.0	93.1
1	1^+	with	65.0	5.0	60.0	60.0	99.9
1	0^-	without	43.4	11.1	32.3	34.4	93.9
1	0^-	with	47.7	13.3	34.4	34.4	99.9
1	1^-	without	114.7	16.1	98.5	103.3	95.4
1	1^-	with	124.3	21.1	103.2	103.3	99.9
1	2^-	without	177.8	13.9	163.9	172.1	95.2
1	2^-	with	194.4	22.3	172.1	172.1	100.0
2	1^+	without	56.6	0.5	56.1	60.0	93.6
2	1^+	with	64.7	4.8	59.9	60.0	99.9
2	0^-	without	47.5	10.0	37.5	39.4	95.2
2	0^-	with	51.4	12.1	39.3	39.4	99.8
2	1^-	without	129.2	15.7	113.5	118.1	96.1
2	1^-	with	138.3	20.5	117.8	118.1	99.7
2	2^-	without	202.9	13.9	188.9	196.9	96.0
2	2^-	with	218.3	21.9	196.4	196.9	99.7

becomes more exhausted with increasing temperature. The reason is that the transition strengths of T^+ channel are suppressed with increasing temperature, as analyzed in Sec. III B, and hence the S_+ becomes smaller. While on the other hand, S_- becomes larger with increasing temperature. However, for the case with Dirac sea, the increase in temperature causes a slight decrease in the exhaustion of non-energy-weighted sum rule (about 0.2%–0.3% from $T = 0$ to 2 MeV), which could be related to the fact that the excitation strengths related to antinucleon degrees of freedom in T^- channel decrease with increasing temperature.

In Figs. 7 and 8, we display the exhaustion of non-energy-weighted sum rule in T^+ channel (defined as the ratio of the strength summation in T^+ channel to the non-energy-weighted sum rule, i.e., $\frac{S_+}{\text{Sum rule}}$) for ^{80}Zn and ^{126}Ru calculated with and without contributions from Dirac sea at different temperatures. It is clear to see that the exhaustion of the non-energy-weighted sum rule for SD$^+$ transitions is remarkably higher than that of GT$^+$ transitions for the case without contributions from the Dirac sea. The strengths for GT$^+$ transitions are almost negligible at different temperatures due to the Pauli blocking effects, as seen from Sec. III B, while the SD$^+$ transitions still have relatively large transition strengths. This indicates that, for the electron-capture cross sections, the first-forbidden SD transitions could play a more important role compared with the allowed GT transitions. The inclusion of the Dirac sea is particularly important for GT$^+$ transitions, which increases its summed transition strength by a factor of nearly 10. Besides, the exhaustion of non-energy-weighted sum rule even decreases with increasing of temperature for both GT$^+$ and SD$^+$ transitions, which is due to the suppression of their transition strength induced by temperature effects, as seen in Sec. III B. Moreover, for SD$^+$ transitions,

TABLE IV. Same as Table III but for the nucleus ^{126}Ru.

T [MeV]	J^π		S_- [fm^2]	S_+ [fm^2]	$S_- - S_+$ [fm^2]	Sum rule [fm^2]	$\frac{S_- - S_+}{\text{Sum rule}}$ [%]
0	1^+	without	106.8	0.9	105.9	114.0	92.9
0	1^+	with	121.4	7.4	114.0	114.0	100.0
0	0^-	without	88.7	8.9	79.8	85.5	93.4
0	0^-	with	97.9	12.5	85.3	85.5	99.9
0	1^-	without	255.4	11.7	243.7	256.4	95.0
0	1^-	with	277.5	21.4	256.1	256.4	99.9
0	2^-	without	415.7	10.9	404.8	427.3	94.7
0	2^-	with	453.5	26.7	426.9	427.3	99.9
1	1^+	without	106.9	0.8	106.1	114.0	93.1
1	1^+	with	121.2	7.3	113.9	114.0	99.9
1	0^-	without	91.0	8.5	82.5	87.8	94.0
1	0^-	with	99.8	12.1	87.7	87.8	99.9
1	1^-	without	261.7	10.6	251.1	263.3	95.3
1	1^-	with	283.3	20.3	263.0	263.3	99.9
1	2^-	without	427.3	9.9	417.4	438.9	95.1
1	2^-	with	464.1	25.7	438.4	438.9	99.9
2	1^+	without	107.3	0.7	106.5	114.0	93.5
2	1^+	with	120.9	7.1	113.7	114.0	99.8
2	0^-	without	103.1	8.4	94.6	99.4	95.2
2	0^-	with	111.2	12.1	99.1	99.4	99.7
2	1^-	without	297.0	11.0	286.1	298.2	95.9
2	1^-	with	317.5	20.3	297.2	298.2	99.7
2	2^-	without	486.6	10.3	476.3	497.0	95.8
2	2^-	with	521.2	25.7	495.4	497.0	99.7

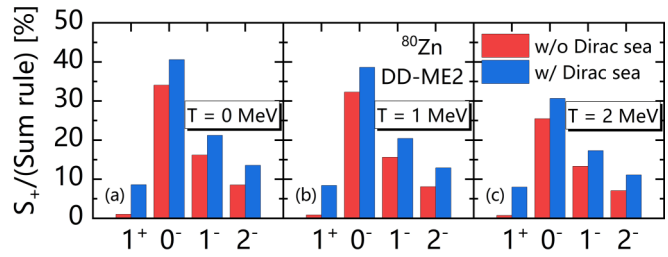

FIG. 7. The exhaustion of non-energy-weighted sum rule of summed transition strengths in T^+ channel for ^{80}Zn, calculated with effective interaction DD-ME2 at $T = 0$, 1, 2 MeV. The results without Dirac-sea contributions (without Dirac sea) and with Dirac-sea contributions (with Dirac sea) are represented by red and blue bars, respectively.

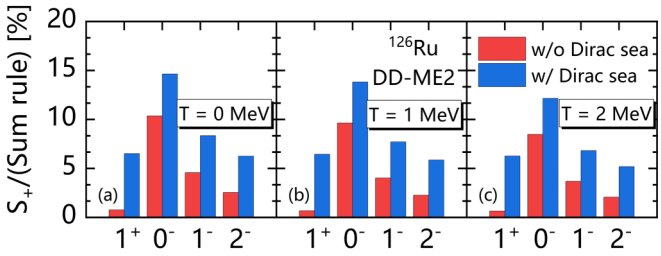

FIG. 8. Same as Fig. 7 but for the nucleus ^{126}Ru.

the exhaustion of non-energy-weighted sum rule also decreases with the increasing multipole J of SD transitions.

IV. CONCLUSIONS

In this work we investigate the GT$^+$ and SD$^+$ transition properties in neutron-rich $N = 50$ nucleus ^{80}Zn and $N = 82$ nucleus ^{126}Ru at $T = 0$, 1, and 2 MeV, based on the self-consistent PNRQRPA model and FT-PNRRPA model. These two nuclei are among the nuclei that have primary contributions to the deleptonization phase of collapse in supernova, as suggested in Ref. [43].

At zero temperature, the GT$^+$ transitions for ^{80}Zn and ^{126}Ru are almost completely Pauli blocked because one more extra shell is occupied for neutrons than that for protons in both nuclei. Therefore, the existing small strengths come from either transitions from the proton intruder orbitals with small occupations induced by pairing correlations, or transitions between orbitals with different node numbers across major shells. In contrast, the SD$^+$ transitions still have relatively large transition strengths, comparing with GT$^+$ transitions through the exhaustion of sum-rule values of T^+ channel.

Upon increasing the temperature to even 2 MeV, the thermal excitation still cannot open up GT$^+$ transitions with high strength because ^{80}Zn and ^{126}Ru are too neutron rich. Instead, the unblocked small GT$^+$ transition strength by pairing correlations even vanishes due to the reversal of particle-like and hole-like properties of corresponding neutron and proton orbitals, caused by the collapse of pairing correlations at high temperatures as well as the thermal excitation of neutron orbitals. Other transitions also become a bit weaker due to the smearing of the Fermi surface at finite temperatures. For the SD$^+$ transitions in ^{80}Zn, the temperature has very small effects both in transition energies and strengths, therefore, the experimental data measured in the laboratory can provide useful information for transitions in an astrophysical environment. However, for SD$^+$ transitions in ^{126}Ru, the transition energies have a decrease of about 2 MeV from zero temperature to $T = 1$ MeV due to the disappearance of pairing gap of the transition orbitals, which could cause an increase of electron-capture cross section because of the increased phase space. In the T^+ channel, the exhaustion of non-energy-weighted sum rule decreases with increasing of temperature for both GT$^+$ and SD$^+$ transitions due to the suppression of their transition strength induced by temperature effects.

It should be noticed that, in this work, the deexcitations which could happen at high temperatures are not considered. These deexcitations for T^+ channel can be obtained by the transitions in T^- channel at negative transition energies [41,52]. Although the GT$^+$ transitions are still blocked at finite temperature in these neutron-rich nuclei, there can be considerable transition strengths at negative energies contributed by deexcitations, which could increase the electron-capture rates by a large amount, as discussed in Ref. [52,72]. Therefore, the further study on electron-capture rates based on spin-isospin excitations at finite temperature is envisaged.

ACKNOWLEDGMENTS

This work is supported by the National Natural Science Foundation of China under Grant No. 12075104 and the "Young Scientist Scheme" of the National Key Research and Development (R&D) Program under Grant No. 2021YFA1601500.

[1] F. Osterfeld, Rev. Mod. Phys. **64**, 491 (1992).
[2] N. Paar, D. Vretenar, E. Khan, and G. Colò, Rep. Prog. Phys. **70**, R02 (2007).
[3] Y. Fujita, B. Rubio, and W. Gelletly, Prog. Part. Nucl. Phys. **66**, 549 (2011).
[4] B. Brown and B. Wildenthal, At. Data Nucl. Data Tables **33**, 347 (1985).
[5] K. Langanke and G. Martínez-Pinedo, At. Data Nucl. Data Tables **79**, 1 (2001).
[6] K. Langanke, E. Kolbe, and D. J. Dean, Phys. Rev. C **63**, 032801(R) (2001).
[7] K. Langanke, G. Martínez-Pinedo, J. M. Sampaio, D. J. Dean, W. R. Hix, O. E. B. Messer, A. Mezzacappa, M. Liebendörfer, H.-T. Janka, and M. Rampp, Phys. Rev. Lett. **90**, 241102 (2003).
[8] Y. F. Niu, N. Paar, D. Vretenar, and J. Meng, Phys. Rev. C **83**, 045807 (2011).
[9] J. N. Bahcall and R. K. Ulrich, Rev. Mod. Phys. **60**, 297 (1988).
[10] H. Dapo and N. Paar, Phys. Rev. C **86**, 035804 (2012).
[11] Janka and Hans-Thomas, Annu. Rev. Nucl. Part. Sci. **62**, 407 (2012).
[12] H.-T. Janka, K. Langanke, A. Marek, G. Martínez-Pinedo, and B. Muller, Phys. Rep. **442**, 38 (2007).
[13] M. Mumpower, R. Surman, G. McLaughlin, and A. Aprahamian, Prog. Part. Nucl. Phys. **86**, 86 (2016).
[14] K. Ikeda, S. Fujii, and J. Fujita, Phys. Lett. **3**, 271 (1963).
[15] R. R. Doering, A. Galonsky, D. M. Patterson, and G. F. Bertsch, Phys. Rev. Lett. **35**, 1691 (1975).
[16] D. Horen, C. Goodman, C. Foster, C. Goulding, M. Greenfield, J. Rapaport, D. Bainum, E. Sugarbaker, T. Masterson, F. Petrovich, and W. Love, Phys. Lett. B **95**, 27 (1980).
[17] C. Gaarde, J. Rapaport, T. Taddeucci, C. Goodman, C. Foster, D. Bainum, C. Goulding, M. Greenfield, D. Horen, and E. Sugarbaker, Nucl. Phys. A **369**, 258 (1981).
[18] S. Hatori, H. Miyatake, S. Morinobu, K. Katori, M. Fujiwara, I. Katayama, N. Ikeda, T. Fukuda, T. Shinozuka, and K. Ogawa, Nucl. Phys. A **549**, 327 (1992).
[19] M. Ichimura, H. Sakai, and T. Wakasa, Prog. Part. Nucl. Phys. **56**, 446 (2006).
[20] L.-J. Wang, Y. Sun, and S. K. Ghorui, Phys. Rev. C **97**, 044302 (2018).

[21] T. Suzuki, R. Fujimoto, and T. Otsuka, Phys. Rev. C **67**, 044302 (2003).
[22] T. Suzuki, M. Honma, H. Mao, T. Otsuka, and T. Kajino, Phys. Rev. C **83**, 044619 (2011).
[23] E. Caurier, G. Martínez-Pinedo, F. Nowack, A. Poves, and A. P. Zuker, Rev. Mod. Phys. **77**, 427 (2005).
[24] A. Pastore, D. Davesne, and J. Navarro, Phys. Rep. **563**, 1 (2015).
[25] T. Nikšć, D. Vretenar, and P. Ring, Phys. Rev. C **66**, 064302 (2002).
[26] K. Langanke and G. Martínez-Pinedo, Rev. Mod. Phys. **75**, 819 (2003).
[27] A. A. Dzhioev, K. Langanke, G. Martínez-Pinedo, A. I. Vdovin, and C. Stoyanov, Phys. Rev. C **101**, 025805 (2020).
[28] N. Paar, G. Colò, E. Khan, and D. Vretenar, Phys. Rev. C **80**, 055801 (2009).
[29] A. F. Fantina, E. Khan, G. Colò, N. Paar, and D. Vretenar, Phys. Rev. C **86**, 035805 (2012).
[30] A. L. Goodman, Nucl. Phys. A **352**, 30 (1981).
[31] E. Khan, N. Van Giai, and N. Sandulescu, Nucl. Phys. A **789**, 94 (2007).
[32] Y. F. Niu, Z. M. Niu, N. Paar, D. Vretenar, G. H. Wang, J. S. Bai, and J. Meng, Phys. Rev. C **88**, 034308 (2013).
[33] E. Yüksel, G. Colò, E. Khan, Y. F. Niu, and K. Bozkurt, Phys. Rev. C **96**, 024303 (2017).
[34] E. Yüksel, G. Coló, E. Khan, and Y. F. Niu, Eur. Phys. J. A **55**, 230 (2019).
[35] A. A. Dzhioev, A. I. Vdovin, and C. Stoyanov, Phys. Rev. C **100**, 025801 (2019).
[36] E. Litvinova, C. Robin, and H. Wibowo, Phys. Lett. B **800**, 135134 (2020).
[37] P. Ring, Prog. Part. Nucl. Phys. **37**, 193 (1996).
[38] J. Meng, H. Toki, S. Zhou, S. Zhang, W. Long, and L. Geng, Prog. Part. Nucl. Phys. **57**, 470 (2006).
[39] A. Ravlić, Y. F. Niu, T. NikNikšić, N. Paar, and P. Ring, Phys. Rev. C **104**, 064302 (2021).
[40] A. Ravlić, E. Yüksel, Y. F. Niu, G. Colò, E. Khan, and N. Paar, Phys. Rev. C **102**, 065804 (2020).
[41] A. Ravlić, E. Yüksel, Y. F. Niu, and N. Paar, Phys. Rev. C **104**, 054318 (2021).
[42] K. Langanke, G. Martínez-Pinedo, and R. G. T. Zegers, Rep. Prog. Phys. **84**, 066301 (2021).
[43] C. Sullivan, E. O'Connor, R. G. T. Zegers, T. Grubb, and S. M. Austin, Astrophys. J. Lett. **816**, 44 (2015).
[44] S. Furusawa, H. Nagakura, K. Sumiyoshi, C. Kato, and S. Yamada, Phys. Rev. C **95**, 025809 (2017).
[45] A. R. Raduta, F. Gulminelli, and M. Oertel, Phys. Rev. C **95**, 025805 (2017).
[46] A. V. Yudin, M. Hempel, S. I. Blinnikov, D. K. Nadyozhin, and I. V. Panov, Mon. Not. R. Astron. Soc. **483**, 5426 (2019).
[47] H. Nagakura, S. Furusawa, H. Togashi, S. Richers, K. Sumiyoshi, and S. Yamada, Astrophys. J., Suppl. Ser. **240**, 38 (2019).
[48] R. Titus, C. Sullivan, R. G. T. Zegers, B. A. Brown, and B. Gao, J. Phys. G **45**, 014004 (2018).
[49] A. Pascal, S. Giraud, A. F. Fantina, F. Gulminelli, J. Novak, M. Oertel, and A. R. Raduta, Phys. Rev. C **101**, 015803 (2020).
[50] R. Titus, E. M. Ney, R. G. T. Zegers, D. Bazin, J. Belarge, P. C. Bender, B. A. Brown, C. M. Campbell, B. Elman, J. Engel, A. Gade, B. Gao, E. Kwan, S. Lipschutz, B. Longfellow, E. Lunderberg, T. Mijatović, S. Noji, J. Pereira, J. Schmitt, C. Sullivan, D. Weisshaar, and J. C. Zamora, Phys. Rev. C **100**, 045805 (2019).
[51] J. C. Zamora, R. G. T. Zegers, S. M. Austin, D. Bazin, B. A. Brown, P. C. Bender, H. L. Crawford, J. Engel, A. Falduto, A. Gade, P. Gastis, B. Gao, T. Ginter, C. J. Guess, S. Lipschutz, B. Longfellow, A. O. Macchiavelli, K. Miki, E. Ney, S. Noji, J. Pereira, J. Schmitt, C. Sullivan, R. Titus, and D. Weisshaar, Phys. Rev. C **100**, 032801(R) (2019).
[52] S. Giraud, R. G. T. Zegers, B. A. Brown, J.-M. Gabler, J. Lesniak, J. Rebenstock, E. M. Ney, J. Engel, A. Ravlić, and N. Paar, Phys. Rev. C **105**, 055801 (2022).
[53] N. Paar, P. Ring, T. Nikšć, and D. Vretenar, Phys. Rev. C **67**, 034312 (2003).
[54] N. Paar, T. Nikšć, D. Vretenar, and P. Ring, Phys. Rev. C **69**, 054303 (2004).
[55] D. Vale, Y. F. Niu, and N. Paar, Phys. Rev. C **103**, 064307 (2021).
[56] A. Juodagalvis, K. Langanke, W. Hix, G. Martínez-Pinedo, and J. Sampaio, Nucl. Phys. A **848**, 454 (2010).
[57] A. L. Goodman, Nucl. Phys. A **352**, 45 (1981).
[58] J. Cooperstein and J. Wambach, Nucl. Phys. A **420**, 591 (1984).
[59] G. A. Lalazissis, T. Nikšć, D. Vretenar, and P. Ring, Phys. Rev. C **71**, 024312 (2005).
[60] J. Berger, M. Girod, and D. Gogny, Nucl. Phys. A **428**, 23 (1984).
[61] C. L. Bai, H. Sagawa, G. Colò, Y. Fujita, H. Q. Zhang, X. Z. Zhang, and F. R. Xu, Phys. Rev. C **90**, 054335 (2014).
[62] C. Bai, H. Sagawa, M. Sasano, T. Uesaka, K. Hagino, H. Zhang, X. Zhang, and F. Xu, Phys. Lett. B **719**, 116 (2013).
[63] Y. K. Gambhir, J. P. Maharana, G. A. Lalazissis, C. P. Panos, and P. Ring, Phys. Rev. C **62**, 054610 (2000).
[64] G. A. Lalazissis, J. König, and P. Ring, Phys. Rev. C **55**, 540 (1997).
[65] Y.F.Niu, N. Paar, D. Vretenar, and J. Meng, Phys. Lett. B **681**, 315 (2009).
[66] A. Krasznahorkay, M. Fujiwara, P. van Aarle, H. Akimune, I. Daito, H. Fujimura, Y. Fujita, M. N. Harakeh, T. Inomata, J. Jänecke, S. Nakayama, A. Tamii, M. Tanaka, H. Toyokawa, W. Uijen, and M. Yosoi, Phys. Rev. Lett. **82**, 3216 (1999).
[67] H. Sagawa, S. Yoshida, X.-R. Zhou, K. Yako, and H. Sakai, Phys. Rev. C **76**, 024301 (2007).
[68] A. A. Dzhioev, A. I. Vdovin, V. Y. Ponomarev, J. Wambach, K. Langanke, and G. Martínez-Pinedo, Phys. Rev. C **81**, 015804 (2010).
[69] Z.-Y. Ma, B.-Q. Chen, N. Van Giai, and T. Suzuki, Eur. Phys. J. A **20**, 429 (2004).
[70] H. Liang, N. Van Giai, and J. Meng, Phys. Rev. Lett. **101**, 122502 (2008).
[71] P. Ring, Z. yu Ma, N. Van Giai, D. Vretenar, A. Wandelt, and L. gang Cao, Nucl. Phys. A **694**, 249 (2001).
[72] E. M. Ney, A. Ravlić, J. Engel, and N. Paar, arXiv:2209.10009.